International Geology Review, Vol. 44, 2002, p. 62–82.

Integrating Geologic and Geodetic Estimates of Slip Rate on the San Andreas Fault System

PAUL SEGALL

Department of Geophysics, Stanford University, Stanford, California 94305

Abstract

Interseismic deformation measurements are generally interpreted in terms of steady slip on buried elastic dislocations. Although such models often yield slip rates that are in reasonable accord with geologic observations, they are inconsistent with our expectation of fault structure at depth, and cannot explain transient postseismic deformation following large earthquakes. An alternate two-dimensional model of repeating earthquakes that break an elastic plate of thickness H, overlying a Maxwell viscoelastic half-space with relaxation time τ_R (Savage and Prescott, 1978) involves five parameters; H, τ_R, t, T, and $\dot{s}$, where t is the time since the last quake, T is the earthquake repeat time, and $\dot{s}$ is the slip rate. Many parts of the San Andreas fault (SAF) system involve multiple parallel faults, which further increases the number of parameters to be estimated. All hope is not lost, however, if we make use of geologic constraints on slip rate, as well as the measured time-dependent strain following the 1906 earthquake, in addition to the present-day spatial distribution of deformation rate.

GPS data from the Carrizo Plain segment of the SAF imply a considerably larger relaxation time than inferred from the post-1906 strain rate transient recorded by repeated triangulation surveys. This may indicate that the simple Savage-Prescott model is deficient, or that the crustal structure and/or thermal profile differs significantly between northern and central California. The data are consistent with an average recurrence interval of ~280 years, which agrees reasonably well with paleoseismic estimates.

To test the effect of regional variations in H and τ_R, I analyze GPS-derived velocities from the northern San Francisco Bay area (Prescott et al., 2001), and include the SAF, the Hayward-Rodgers Creek (HRC), and Concord-Green Valley faults (CGV). Optimization using constrained non-linear least squares yields: H ~18 km, τ_R ~35 years, T_{SAF} = 280 years, $\dot{s}_{SAF}$, ~25 mm/yr, t_{HRC} = 225 years, T_{HRC} = 429 years, and $\dot{s}_{HRC}$ ~7 mm/yr. The effect of the Concord–Green Valley faults is modeled kinematically; the optimal model involves 8 mm/yr of slip beneath 2 km. While neither the average recurrence interval on the SAF or HRC is well resolved, the optimal inter-event time for the SAF is in reasonable agreement with paleoseismic results, which indicate that the most recent event prior to 1906 occurred in the mid-1600s. The geodetic data also favor the latest date allowed by historical data (~1775) for the most recent HRC earthquake, a result not inconsistent with the paleoseismic finding that the most recent event there occurred in the interval 1670–1776. The conclusion of this study is that by combining the present-day deformation field, post-1906 strain data, and geologic bounds on slip rate and maximum earthquake slip, it is possible to estimate parameters of considerable geophysical interest, including time since the most recent earthquake and average recurrence intervals.

Introduction

INTERSEISMIC DEFORMATION DATA collected along the San Andreas fault system reveals a broad zone of strain that extends roughly 100 km perpendicular to the strike of the principal faults (e.g., Johnson et al., 1994). Approximately 35 mm/yr of relative displacement is accommodated across this region (e.g., Prescott et al., 2001). Geodetic strain data such as these are important components of seismic hazard evaluations. Simply stated, the higher the strain rate the bigger, or more frequent, the earthquakes must be to relieve that strain. More quantitative information about earthquake occurrence can only be made through reference to a mechanical model of the deformation field. The simplest, and most widely used, model is that of an infinitely long screw dislocation in an elastic half-space introduced by Savage and Burford in 1970. In this case the

fault parallel velocity $v(x)$, is a simple function of slip rate $\dot{s}$ and the fault locking depth d, $v(x) = (\dot{s}/\pi)\tan^{-1}(x/d)$. Here x is distance normal to the fault. Given measured velocities $v(x_i)$, it is straightforward to estimate that depth over which faults are locked, and the average slip rate across those faults (e.g., Williams et al., 1994). This approach has been generalized for finite length dislocations (e.g., Matsu'ura et al., 1986) and for far-field motions consistent with rigid spherical plates (e.g., Murray and Segall, 2001). Slip rates estimated from geodetic observations can be compared to those derived from geologic studies, and along with the average slip in large earthquakes form the basis of seismic hazard evaluations.

The screw dislocation, while a useful first-order model of plate boundary deformation, does not accurately represent fault structure at great depth within the earth. Nor does it account for temporal variations in strain rate that have been observed following large earthquakes. More physically realistic models tend to fall into two categories. The first involves faulting in an elastic lithosphere overlying a viscoelastic lower crust or upper mantle (Nur and Mavko, 1974; Savage and Prescott, 1978; Lehner et al., 1981; Cohen, 1982; Rundle, 1986; Lyzenga, 1991; Pollitz, 1992). The viscoelastic medium may extend to great depth, or be limited to a channel of finite thickness. Some studies have investigated non-linear rheology (e.g., Reches et al., 1994). The second class of models explains time-dependent deformation following earthquakes as arising from velocity strengthening slip on a downdip extension of the coseismic fault surface (e.g., Tse and Rice, 1986). Most of these models can fit the present-day distribution of strain rate across the San Andreas fault system with an appropriate choice of parameters. A significant complexity in applying these models, however, is the fact that in many places the San Andreas fault system consists of multiple parallel faults. In the San Francisco Bay region, we have the San Andreas, Hayward–Rodgers Creek, and the Calaveras–Concord–Green Valley faults. In southern California, the subparallel Elsinore and San Jacinto faults are present, in addition to the San Andreas. Because physically realistic models of faulting invariably involve a large number of parameters and are slower to compute, they are not often used in inversions of geodetic measurements. Furthermore, Savage (1990) has shown that it is difficult to distinguish between these two classes of models, because the solution for the anti-plane viscoelastic problem has a corresponding elastic solution involving time-dependent slip below the coseismic rupture. The latter two observations have led to the feeling that more physically realistic models are unwarranted.

In this paper, I argue that a key to moving forward with this problem is to include more information than simply the present-day deformation field. Additional information comes from the time dependence of deformation following large earthquakes, and paleoseismic estimates of fault slip rates. *A priori* information about faultslip rate from geologic studies can be used to complement information from geodetic studies. In the present paper, this is done in the context of rather simple models of the earthquake cycle involving repeated earthquakes in an elastic layer overlying a Maxwell viscoelastic half-space. Although this model is itself highly idealized, the results are sufficiently encouraging to warrant further investigations.

The use of *a priori* information to regularize an ill-posed inverse problem is well known (e.g., Jackson, 1979; Tarantola and Valette, 1982; Menke, 1989). In this work, I propose using Bayes' rule to combine geologic and geodetic information, in order to permit use of more sophisticated, and hopefully realistic, models than could be addressed with geodetic data alone. Previously, Minster and Jordan (1987) used Bayes' rule to combine geodetic and geologic data to estimate the net motion across the San Andreas fault system. The general framework proposed here could be expanded to include information from other data sets as well, but the focus here is on slip-rate data. Fault slip rates are determined from geologic observations such as measurements of offset stream channels and dates of the correlative sedimentary deposits. From the point of view of geodetic analysis, this information places *a priori* constraints on the slip rate. I denote the probability density function (p.d.f.) of the slip rate from the geologic observations as $P(\dot{s})$, or perhaps more appropriately as $P(\dot{s}|g)$, where g denotes geologic observations such as measured offsets, radiometric age determination,and so forth.

On the other hand, mechanical models of the earth allow us to predict geodetic observations given the slip rate on the fault and the other model parameters such as the fault locking depth, elastic-layer thickness, viscosity of the lower crust, and so forth. Denoting the parameters of the mechanical model other than slip rate as **m**, then the model yields

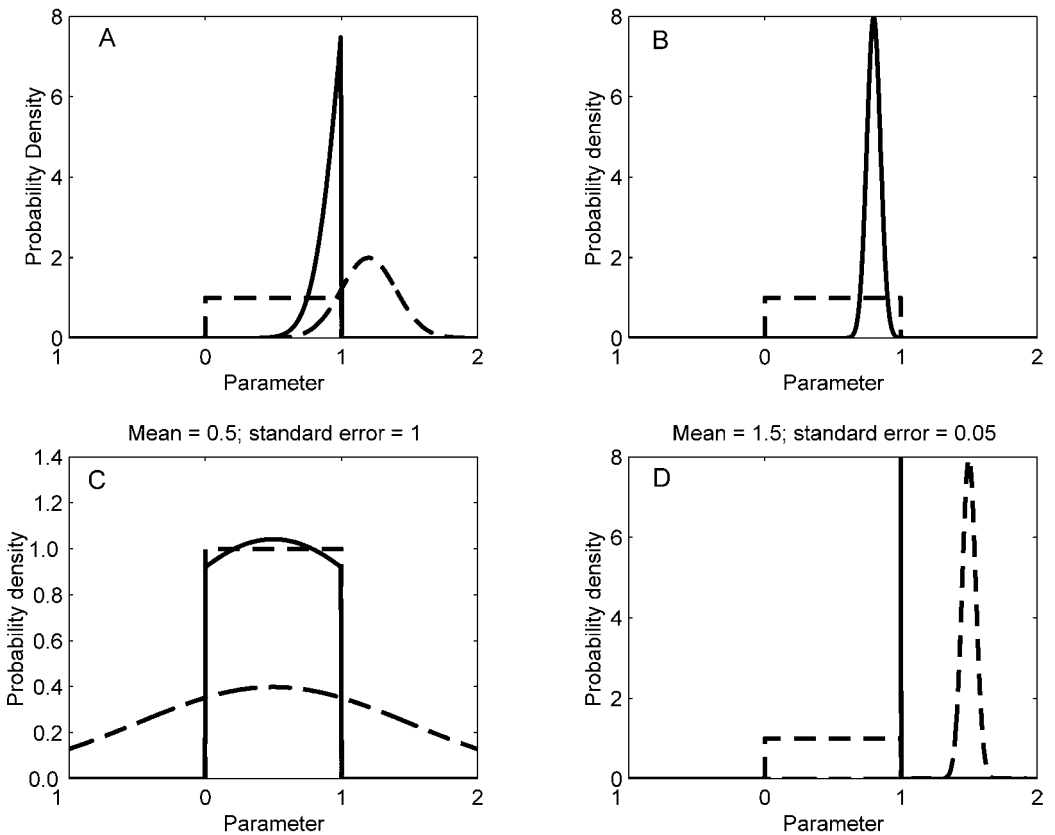

FIG. 1. Example of application of Bayes' theorem given a uniform prior distribution. The prior distribution is uniform over the interval [0,1], and is shown in the dash-dot pattern. The distribution from the data alone is dashed, and the posterior distribution is solid. In (D) the posterior distribution is essentially a delta function at 1.0.

$P(\mathbf{d}|\dot{s}, \mathbf{m})$, where $\mathbf{d}$ is a vector of geodetic data. Bayes' rule then states that

$$P(\dot{s}, \mathbf{m}|\mathbf{d}) = \frac{P(\dot{s}, \mathbf{m})P(\mathbf{d}|\dot{s}, \mathbf{m})}{\int_{s,\,\mathbf{m}} P(\dot{s})P(\mathbf{d}|\dot{s}, \mathbf{m})\, d\dot{s}\, d\mathbf{m}}. \quad (1)$$

In words, equation (1) states that the p.d.f. of the slip-rate and fault-model parameters, given geodetic observations, can be determined from the *a priori* distributions of the slip-rate and the fault-model parameters, and the theoretical model linking the parameters to the geodetic observations. The integral in the denominator ensures that the *posterior* probability is properly normalized, i.e. that the cumulative probability is unity. Assuming that the prior probability of the slip rate and the model parameters are independent, then $P(\dot{s}, \mathbf{m}) = P(\dot{s})P(\mathbf{m})$. This is reasonable inasmuch as estimates of slip rate from paleoseismic studies are independent of prior estimates of elastic layer thickness, viscosity, fault locking depth, and so on. While, in general, we have *a priori* constraints on these physical parameters for the purposes of the present discussion, I will often assume that the distribution is so broad as to be non-informative. Given the independence of the prior distributions on s and m, (1) reduces to

$$P(\dot{s}, \mathbf{m}|\mathbf{d}, \mathbf{g}) = \frac{P(\dot{s}|\mathbf{g})P(\mathbf{m})P(\mathbf{d}|\dot{s}, \mathbf{m})}{\int_{s,\,\mathbf{m}} P(\dot{s}|\mathbf{g})P(\mathbf{m})P(\mathbf{d}|\dot{s}, \mathbf{m})\, d\dot{s}\, d\mathbf{m}}. \quad (2)$$

The posterior probability distribution is easily computed if the prior distribution is uniform over some range. That is, we take the slip rate to be equally probable between specified upper and lower bounds. A simple illustration (Fig. 1) can be informative. In Figure 1A, the mean of the distribution falls just outside the *a priori* bounds. The posterior distribution is thus highly concentrated near the upper bound from geologic data. The geodetic and

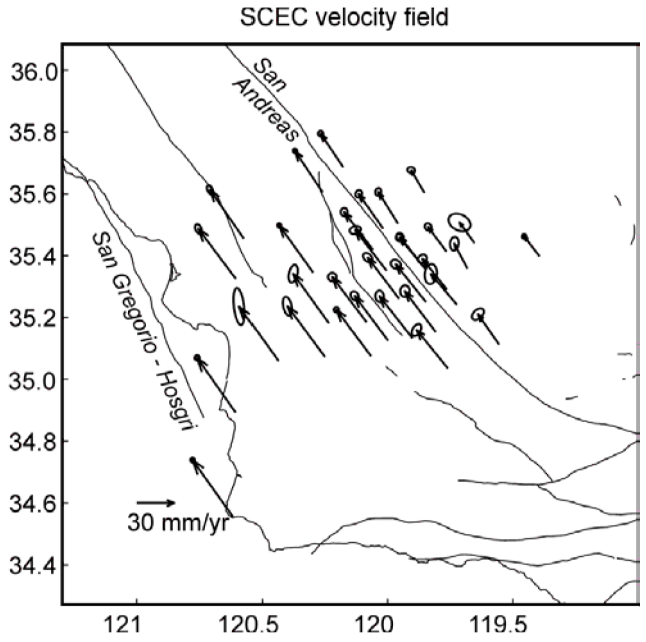

FIG. 2. Velocities determined by the Southern California Earthquake Center (SCEC) in the Carrizo Plain section of the San Andreas fault.

geologic data together are much more informative than either data set alone. In Figure 1B, the *a priori* bounds are so broad as to be uninformative; the posterior distribution is equal to that obtained from the geodetic data alone. In Figure 1C, the reverse is true; the geodetic data supply little information and the posterior distribution reflects simply the *a priori* information. A fourth outcome also is possible, as illustrated in Figure 1D, where the two distributions do not overlap, indicating that the two estimates are inconsistent. The conclusion in this case is that either the uncertainties in the geologic determination of slip rate have been substantially mis-estimated, or the physical model used to relate geodetic data to slip rate is invalid. The outcome in Figure 1D could be the most useful in that, assuming the geologic bounds are valid, it would invalidate an entire class of physical fault models.

I start by considering the interseismic velocity distribution across the Carrizo Plain segment of the San Andreas fault (Fig. 2). This area is chosen because it is the simplest part of the SAF system, uncomplicated by parallel faults. The only other active structures at this latitude are the San Gregorio–Hosgri fault system, which runs into an active deformation zone in the Santa Maria Basin (Feigl et al., 1990), and the fold-and-thrust belt northeast of the San Andreas at the eastern edge of the Coast Ranges. The latter structures involve motion largely normal to the SAF and thus do not significantly affect the calculations here. The San Gregorio–Hosgri deformation is accounted for, crudely, using a simple dislocation model.

Assuming only a single San Andreas fault, and making use of a two-dimensional dislocation model, I find that the best-fitting locking depth is 24.4 km (Fig. 3), and the slip rate is 41.8 mm/yr. In contrast, Sieh and Jahns (1984) determined an average slip rate of 33.9 ± 2.9 mm/yr for the past 3,700 yr, and 35.8 + 5.4/–4.1 mm/yr for the past 13,250 yr, based on offset fluvial deposits at Wallace Creek. Allowing 3 mm/yr of slip on the San Gregorio–Hosgri fault system, which is modeled as a screw dislocation locked above 10 km, the San Andreas locking depth shallows slightly to 20.3 km, and the slip rate drops to 37.7 mm/yr, which is in reasonable accord with geologic estimates (Sieh and Jahns, 1984).

Of course, the San Andreas fault is not two-dimensional. Southeast of the Carrizo Plain the San Andreas fault enters the Big Bend and the Transverse Ranges, whereas the creeping zone is located to the northwest. The data analyzed here (Fig. 2) were selected to be as far from possible from these locales, yet some bias is unavoidable with a two-dimensional model.

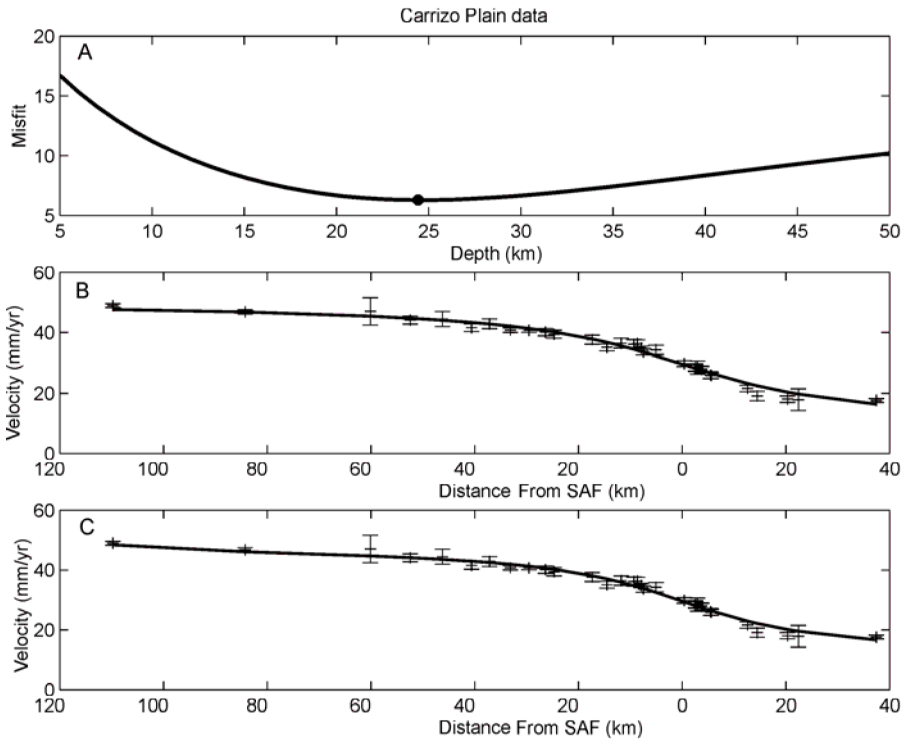

FIG. 3. A. Misfit as a function of depth for a simple screw dislocation model. B. Profile of fault parallel velocity across the fault, compared with prediction of a simple screw dislocation model. C. As in (B) but with 3 mm/yr of slip beneath the Hosgri fault.

It is important to determine the range of slip rates and locking depths that are consistent with the GPS data. A bootstrap resampling procedure shows that slip rates in the range of 34 to 41 mm/yr are consistent with the geodetic observations (Fig 4). The bootstrap was conducted in the following manner: Let $\mathbf{d}$ be the vector of observations, $\hat{\mathbf{d}}$ the predicted data from the best-fitting model, so that $\mathbf{r} = \mathbf{d} - \hat{\mathbf{d}}$ is the vector of residuals. The residuals were randomly resampled with replacement; that is, some elements may be chosen multiple times, others not at all. Denote the resampled residuals $\mathbf{r}^*$. A resampled data vector, $\mathbf{d}^* = \hat{\mathbf{d}} + \mathbf{r}^*$, is then used to generate a model estimate and the process is repeated many times. The distribution of the bootstrapped model parameters is that shown in Figure 4.

It is well known that there is a tradeoff between the locking depth and deep slip rate. Increasing the locking depth moves the dislocation farther from the surface observation stations; to achieve the same surface strain requires a higher slip rate. Applying *a priori* constraints on the slip rate, from 31 mm/yr and 37 mm/yr based on the Sieh and Jahns (1984) data from Wallace Creek, thus not only changes the posterior distribution of slip rate, but of the locking depth as well (Fig. 5). The reason for this can be clearly seen from a scatter plot of the bootstrap resamples as in Figure 6.

Notice that the GPS data have significantly narrowed the distribution of admissible slip rates (Fig. 5). The posterior distribution is peaked at 35 to 37 mm/yr, whereas the *a priori* distribution is uniform between 31 and 37 mm/yr. At the same time, the *a priori* geologic information provided no constraint on the fault locking depth. With geologic data alone, we cannot distinguish between a locked fault and a fault that creeps steadily below some shallow locked interval. The GPS data alone bound the locking depth to between 17 and 24 km. Because of the strong correlation between slip rate and locking depth, the posterior distribution of the locking depth is narrowed to 17–20 km. This simple example shows the power of using *a priori* geologic constraints in allowing more information to be obtained from geodetic data.

Note that the bootstrap provides an estimate of the distribution of the model parameters, whereas Bayes' rule requires $P(\mathbf{d}|\mathbf{m})$, as in equation (3). However, for linear models with normally distrib-

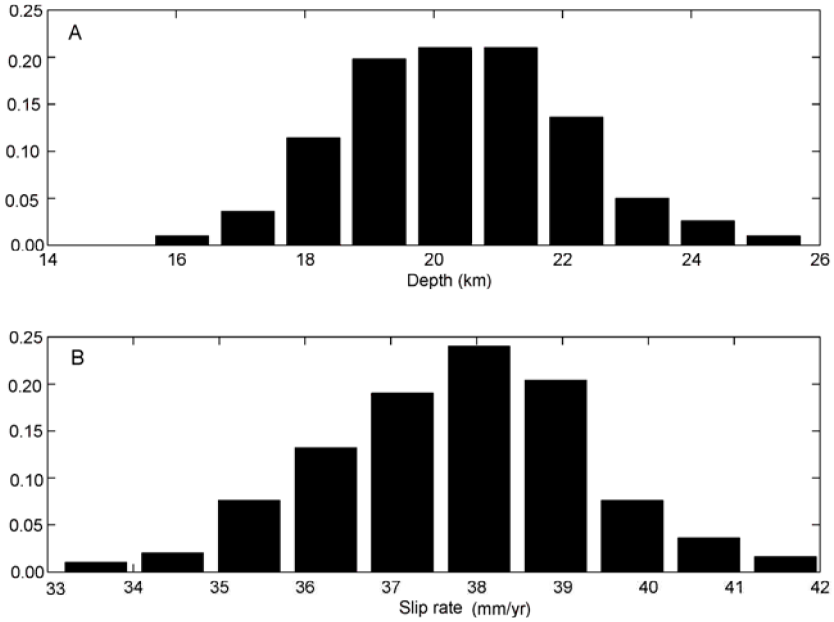

FIG. 4. Probability distributions for fault locking depth and slip rate from bootstrap results using GPS data. I assume 3 mm/yr below a locking depth of 10 km on the Hosgri fault system.

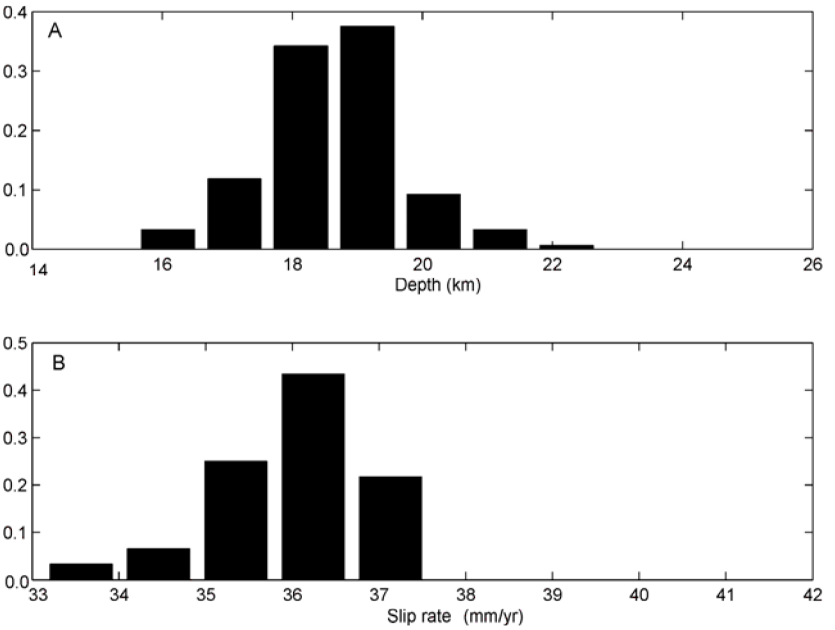

FIG. 5. Posterior probability distribution from the bootstrap results using GPS data and assuming a uniform priordistribution on slip rate from 31 to 37 mm/yr. Compare with Figure 4. As before, I assume 3 mm/yr below a locking depth of 10 km on the Hosgri fault system.

uted observational errors, the two approaches are equivalent. Furthermore, a uniform distribution with hard bounds may not be the best characterization of the prior probability distribution on slip rate. Alternatively, if the prior distribution and observational errors are normally distributed, one can simply apply the prior information as "pseudo data" (e.g., Jackson, 1979).

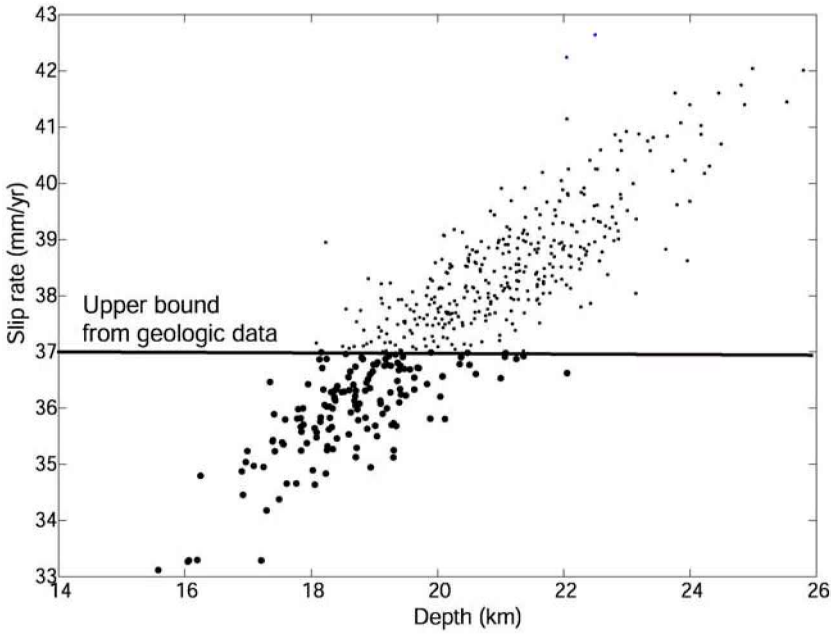

FIG. 6. Tradeoff between slip rate and locking depth. Each point is the result of a bootstrap resample of the SCEC velocity data. The heavy points are those consistent with a uniform prior distribution on slip rate from 31 to 37 mm/yr. As before, I assume 3 mm/yr below a locking depth of 10 km on the Hosgri fault system.

Viscoelastic Models

As noted in the Introduction, the screw dislocation provides only a very limited description of plate-boundary faulting. A somewhat more realistic model involves an elastic layer of thickness H overlying a Maxwell viscoelastic half-space (Fig. 7). The Maxwell material has relaxation time $\tau_R = 2\eta/\mu$, where η is the viscosity and μ is the shear modulus. At time $t = 0$ slip Δu occurs on the fault from the surface to depth $D \le H$. The velocity on the Earth's surface as a function of position perpendicular to the fault, x, and time, t, is

$$v(x,t) = \frac{\Delta u}{\pi\tau_R} e^{-t/\tau_R} \sum_{n=1}^{\infty} \frac{(t/\tau_R)^{n-1}}{(n-1)!} F_n(x, D, H), \quad (3)$$

where the spatial distribution is given by

$$F_n(x, D, H) = \left[\tan^{-1}\left(\frac{D+2nH}{x}\right) + \tan^{-1}\left(\frac{D-2nH}{x}\right)\right] = \tan^{-1}\left[\frac{2xD}{x^2 + (2nH)^2 - D^2}\right]. \quad (4)$$

The result follows from, but is not stated in, Nur and Mavko (1974). The strain rate is simply obtained by differentiating the velocity with respect to x. Notice that the post-seismic velocity is a function of the coseismic slip Δu, the depth of faulting D, the elastic layer thickness H, the material relaxation τ_R, and the time since the last large earthquake t. Equation (3) does not include the effects of interseismic strain accumulation. Savage and Prescott (1978) extended the model by summing over an infinite sequence of plate rupturing events ($D = H$) equally spaced in time with recurrence interval T. The velocity field as a function of distance across strike (x) and time (t) is given by

$$v(x,t) = \frac{\dot{s}}{\pi} \sum_{n=1}^{\infty} T_n(t/\tau_R, T/\tau_R) F_n(x, H, H), \quad (5)$$

where the temporal dependence depends only on the dimensionless ratios t/τ_R and T/τ_R

$$T_n(t/\tau_R, T/\tau_R) = \frac{T}{\tau_R} \frac{e^{-t/\tau_R}}{(n-1)!} \sum_{k=0}^{\infty} e^{-kT/\tau_R} \left(\frac{t+kT}{\tau_R}\right)^{n-1}. \quad (6)$$

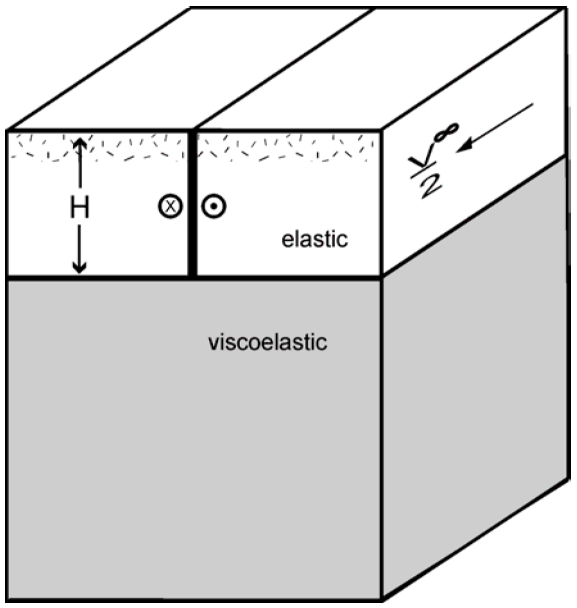

FIG. 7. Model of a faulted elastic plate overlying viscoelastic half-space. The elastic layer has shear modulus μ, the viscoelastic half-space shear modulus μ, and viscosity η. Earthquakes occur at a regular interval T such that the far-field velocity is v∞/2.

Because the far-field lithospheric velocity is driven solely by the repeating earthquakes, $\dot{s} = \Delta u / T$. Representative examples are given in Figure 8 for various times through the earthquake cycle. Notice that when the asthenospheric relaxation time is of the order of the earthquake cycle time or longer, $T/\tau_R \leq 1$, the surface velocity distribution is rather steady with time (Fig. 8A). On the other hand, if the relaxation time is short compared to the recurrence interval $T/\tau_R > 1$, there is a significant transient with higher than average strain rates early in the cycle, and lower than average strain rates late in the cycle.

The Savage-Prescott model involves five parameters: lithospheric thickness H, relaxation time τ_R, time since the last earthquake t, recurrence time T, and long-term slip rate on the fault $\dot{s}$. Because the theory is linear, it is straightforward to construct models with multiple parallel faults; however in this case the number of parameters is even larger. For three faults there are 11 parameters, if one assumes that the elastic thickness and relaxation time are the same for all faults. Note that the model is kinematic, with imposed slip events on the various faults at regular intervals, and thus does not account for the stress interactions between the faults.

As a starting point I consider the Carrizo Plain data with some of the parameters constrained by independent observations. The time since the last great earthquake (1857) is t = 136 years. To begin with, I assume a recurrence time of T = 160 years based on the average interval found by Grant and Sieh (1994). There are three remaining parameters to be estimated from the data: τ_R, H, and $\dot{s}$. The optimal estimates of the non-linear parameters, τ_R, and H, are found by simple grid search (Fig. 9), with $\dot{s}$ estimated by linear least squares. The optimal model is found for H = 11.4 km and τ_R = 80 years, with a slip rate of 40.2 mm/yr. There is a strong tradeoff between relaxation time and elastic-layer thickness, such that models with elastic-layer thickness of up to 20 km and relaxation time of 180 years fit the data nearly equally well. The reason for the tradeoff is as follows: Larger values of H cause the deformation to be spread out in space. At the same time, the deformation becomes more diffuse with increasing t/T and T/τ_R (Fig. 8), and hence $t/\tau_R = (t/T) \cdot (T/\tau_R)$. Thus, decreasing t/τ_R causes the deformation to bemore localized, which counters the effect of increasing H. Interestingly, the slip rate does not vary with H and τ_R, confirming that this parameter is well constrained by the data (given that all other parameters are fixed).

The inferred slip rate is, however, higher than estimated from stream offsets at Wallace Creek of 33 ± 3 mm/yr (Sieh and Jahns, 1984). Constraining the slip rate to 34 mm/yr (Fig. 10) does not fit the data as well, especially for the stations farthest west of the San Andreas. The optimal model is H = 11.4 km as before, but the relaxation time increases to 180 years.

Relaxation times $\tau_R > 50$ years are long compared to what has been inferred for the post-1906 strain rate transient north of the San Francisco Bay as measured by repeated triangulation surveys (Thatcher, 1975a, 1975b; Kenner and Segall, 2000). The relaxation time τ_R consistent with the post-1906 transient can be inferred from the triangulation data and the spatial derivative of equation (3). It would be most consistent to employ the same Savage-Prescott model as used with the Carrizo Plain data; however, this requires knowing the recurrence time of large earthquakes on the north coast segment of the San Andreas fault. An alternate approach employed here is to remove the estimated secular deformation using a model (see Kenner and Segall, 2001) and then fit the remaining strain rate data. For 6.0 meters of slip in the 1906 earthquake, the optimal

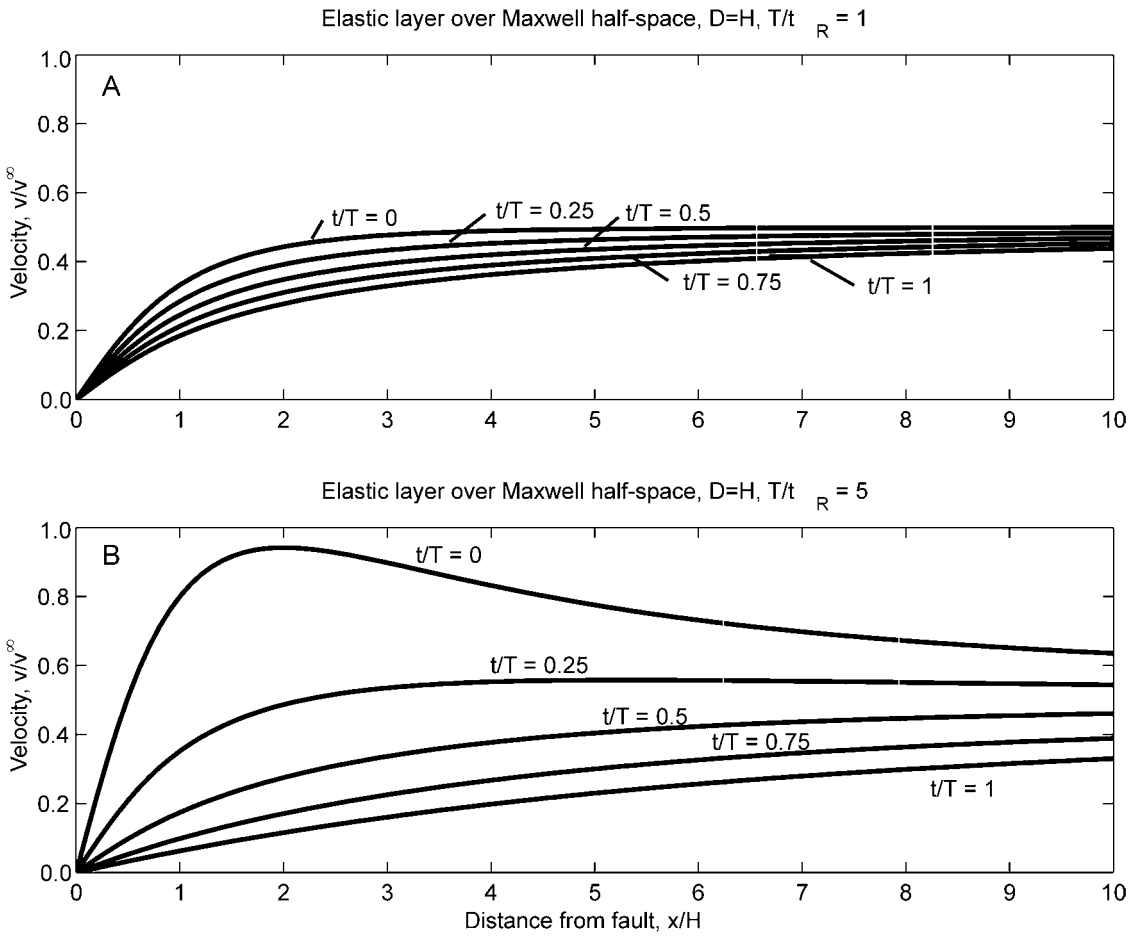

FIG. 8. Savage-Prescott model for (A) $T / \tau_R = 1$, and (B) $T / \tau_R = 5$; t is the time since the last earthquake, T is the earthquake repeat time, and τ_R is the Maxwell relaxation time. In these calculations, the earthquakes rupture the entire elastic layer.

model is H = 19 km with a relaxation time of 17 years (Fig. 11), substantially less than found from the Carrizo Plain interseismic data.[1]

A tentative conclusion of this analysis is that the Carrizo Plain interseismic data require a relaxation time in excess of 50 years, whereas the post-1906 triangulation data require relaxation times of 25 years or less. In order to test whether this discrepancy is truly required by the data, I estimated the uncertainty in the two relaxation times using a bootstrap resampling procedure. As discussed previously, the residuals to the best-fitting model were randomly resampled, with replacement, and added to the model predictions for each bootstrap resample. This approach seems best for small data sets and ensures that there were data at each observation position (interseismic data) and time (postseismic data).

For the post-1906 transient, admissible relaxation times range from 10 years to 30 years (Fig. 12). On the other hand, the present distribution of deformation on the Carrizo Plain demands relaxation times in excess of 35 years (Fig. 13). Thus, we can safely conclude that there is no single relaxation time that fits both data sets.

There are a number of possible explanations for this apparent discrepancy. One possibility is that the model of a fully ruptured elastic plate overlying a linear Maxwell half-space does not capture all of the relevant physics. For example, nonlinear rheology may be important. The data are consistent with the expectation that the effective viscosity is low

[1] Note that the discrepancy is not due to the correction for interseismic deformation in the post-1906 data. Assuming a recurrence time of 250 years and a slip rate on the SAF of 25 mm/yr, the optimal relaxation time is 22.8 years, with an elastic-layer thickness of 16.7 km.

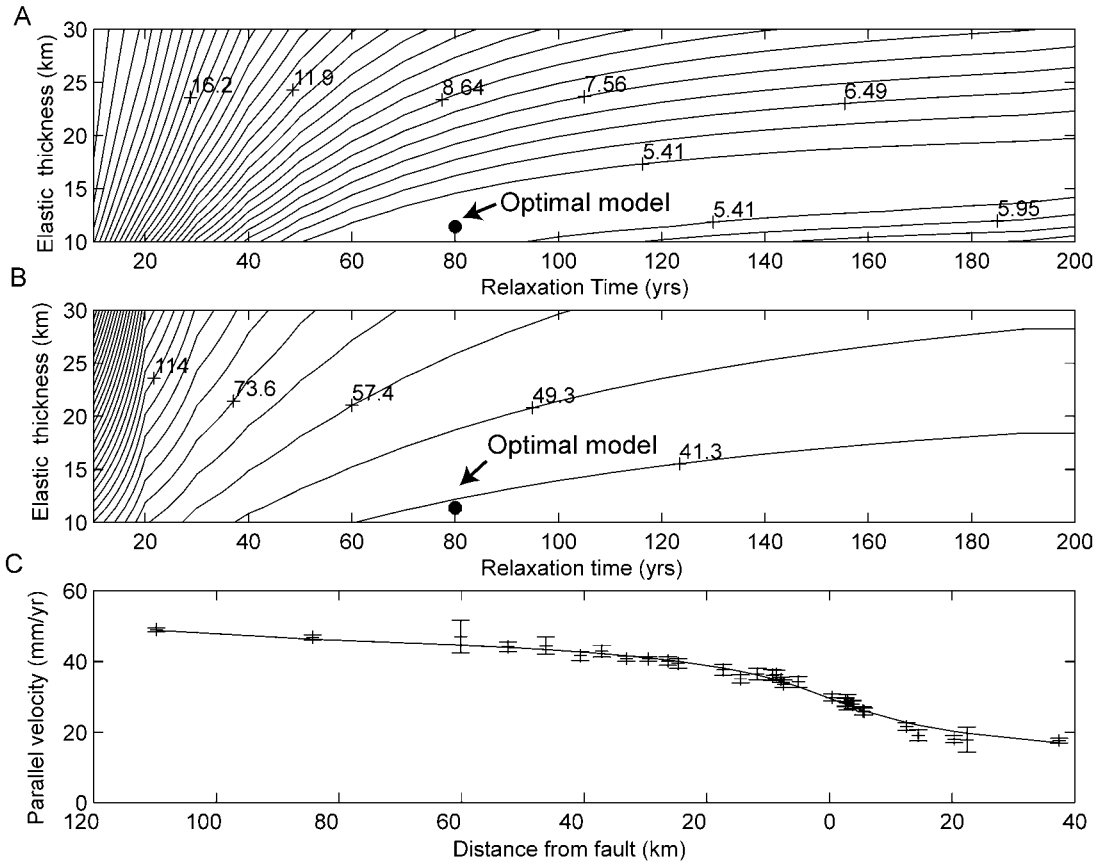

FIG. 9. Comparison of Savage-Prescott model to the SCEC velocity data for the Carrizo Plain. A. Misfit as a function of elastic-layer thickness and relaxation time. B. Best-fitting San Andreas slip rate corresponding to the elastic-layer thickness and relaxation time. C. Fit to the data. Effect of the Hosgri fault is removed employing a dislocation model with slip rate of 3 mm/yr and depth of 10 km.

early in the seismic cycle when the stresses are large, and increases late in the cycle when the stresses have largely dissipated. In addition, recent reflection and refraction results in northern California show the San Andreas fault cutting the lower crust and possibly the Moho (e.g., Henstock et al., 1997; Parsons and Hart, 1999). Aseismic slip on the downdip extension of the seismogenic zone (as in Tse and Rice, 1986) may take place in addition to a more deeply distributed relation. Results from Kenner and Segall (2001), which include viscous relaxation in a narrow fault zone and more deeply distributed slip, find the spatiotemporal pattern of deformation in the post-1906 triangulation data is best fit with a short relaxation time in the fault zone and a longer relaxation in the underlying half-space. Another possibility is that the thermomechanical structure of the lithosphere differs between the two areas. It is also possible that alongstrike variations in fault geometry (the Big Bend) or slip behavior (the creeping zone) may bias the computed relaxation time, although this seems less likely.

Although the apparent relaxation times differ between the Carrizo Plain and the northern San Francisco Bay region, the elastic-layer thickness estimates are consistent in the range of 13–20 km. Carrizo Plain slip-rate estimates cluster near the upper bound of 37 mm/yr. Interestingly, the Carrizo Plain data yield recurrence times greater than 160 years. Whereas the distribution is reasonably broad, both the mean (288 years) and median (277) repeat times fall between the 1988 working group estimate of 296 years (WGCEP, 1988), and the 1995 working group estimate of 206 years (WGCEP, 1995). The average coseismic slip for the predicted events is roughly 10 meters. There are significant correlations between parameters (between H and τ_R, as discussed previously, as well as between τ_R and T), which means that any additional data that constrain

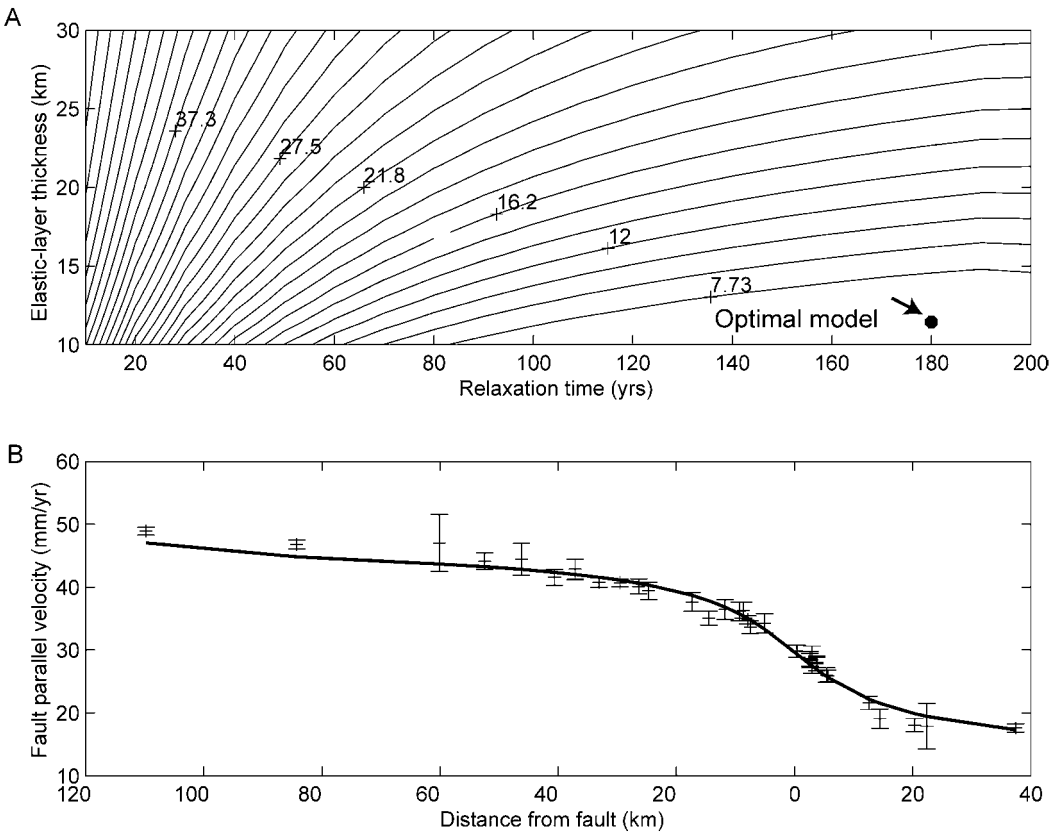

FIG. 10. Comparison of Savage-Prescott model to the SCEC velocity data for the Carrizo Plain with slip rate constrained to 34 mm/yr. Effect of San Gregorio–Hosgri fault has been removed with a dislocation model with slip rate of 3 mm/yr and depth of 10 km. A. Misfit as a function of elastic-layer thickness and relaxation time. B. Fit to the data.

some of the parameters will help resolve others as well.

It should be emphasized that the paleoseismic observations of Grant and Sieh (1994) show an irregular pattern of earthquakes that cannot be explained by the simple two-dimensional model used here to interpret the geodetic observations. Nevertheless, it is interesting that the GPS data appear to have some resolving power for average recurrence interval.

San Francisco Bay Data

In order to eliminate any geographic bias in the interpretation associated with possibly different crustal structure and temperature distribution, I next consider the velocity profile across the San Andreas fault north of the San Francisco Bay as determined by repeated GPS observations (Prescott et al., 2001), as shown in Figure 14. The GPS sites are sufficiently close to the post-1906 triangulation networks that it is reasonable to assume that the crustal structure and thermal profile are the same for both data sets. In the following, the GPS-derived velocities are rotated into fault-parallel and perpendicular components. Only the fault-parallel motions are modeled here, although as pointed out by Prescott et al. (2001), and Murray and Segall (2001), there is significant fault-normal motion in the eastern coast ranges at the western edge of the Central Valley.

The model is the same as discussed previously with three principal faults: the San Andreas, Hayward–Rodgers Creek, and Concord–Green Valley faults. The parameters are the elastic plate thickness H, Maxwell relaxation time τ_R, the recurrence time for great earthquakes on the SAF T_{SAF}, the slip rate on the SAF $\dot{s}_{SAF}$, and the recurrence time T_{HRC}, time since past event t_{HRC}, and slip rate $\dot{s}_{HRC}$ on the Hayward-Rodgers Creek fault system. The time since the last great earthquake on the northern San Andreas fault, t_{SAF} is, of course, known. The effect of the Concord–Green Valley fault is modeled

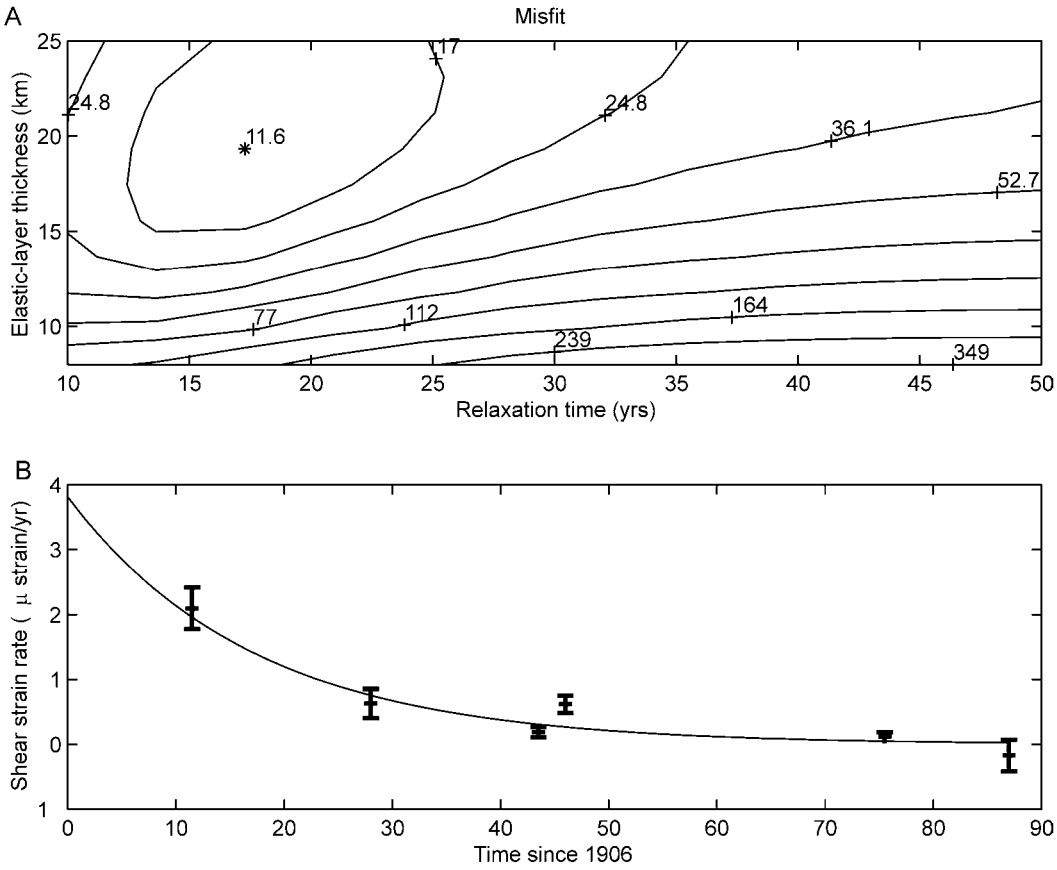

FIG. 11. Post-1906 strain rate from triangulation data in the San Francisco Bay area. Model fit to the model with postseismic deformation only. A. Misfit as a function of elastic-layer thickness and relaxation time. B. Fit to the data.

kinematically with a simple screw dislocation, which adds two parameters: the fault slip rate and locking depth. It is certainly inconsistent to ignore viscoelastic effects for the Concord–Green Valley fault, but I do so for three reasons: (a) much less is known about this fault; (b) earthquakes there are presumably least well modeled by infinitely long ruptures; and (c) it keeps the number of parameters reasonably tractable. In essence, the effect of the Concord–Green Valley is removed empirically, and I make no attempt to gain further insights into its mechanical behavior. Future work should address, and hopefully rectify, this simplification.

A priori bounds on the parameters are listed in Table 1. The lower bound on the lithospheric thickness comes from a conservative estimate of the depth extent of slip in large earthquakes. In fact, it is more likely that slip in 1906 extended at least to 15 km (Matthews and Segall, 1993), as it certainly did in the Loma Prieta earthquake (e.g., Beroza, 1991). The bounds on relaxation time come from the preliminary analysis above (Figs. 12 and 13). The lower bound on T_{SAF} comes from the elapsed time since 1906, the upper bound from limits on the amount of coseismic slip (see below). The lower bounds on t_{HRC} and T_{HRC} are derived from the historical record; there is no known earthquake on the northern Hayward–Rodgers Creek system since at least 1775 (Toppozada and Borchardt, 1998; WGCEP, 1999). The lower and upper bounds on slip rates were based loosely on the Northern California Working group (WGCEP, 1999, Table 2). The Working Group listed 2 σ uncertainties of: $\dot{s}_{SAF} = 24 \pm 3$ mm/yr, $\dot{s}_{HRC} = 9 \pm 2$ mm/yr, and $\dot{s}_{HRC} = 5 \pm$ m 3 mm/yr.

The estimation problem is to find the choice of the nine parameters in Table 1 that minimize the misfit to two geodetic data sets: the present-day spatial distribution of deformation in the north San Francisco Bay region (Fig. 14), and the time-dependent decay in strain rate following the 1906 earthquake (Fig. 11). For a non-linear problem such as this, one always needs to be concerned about local minima. However, preliminary testing with a simu-

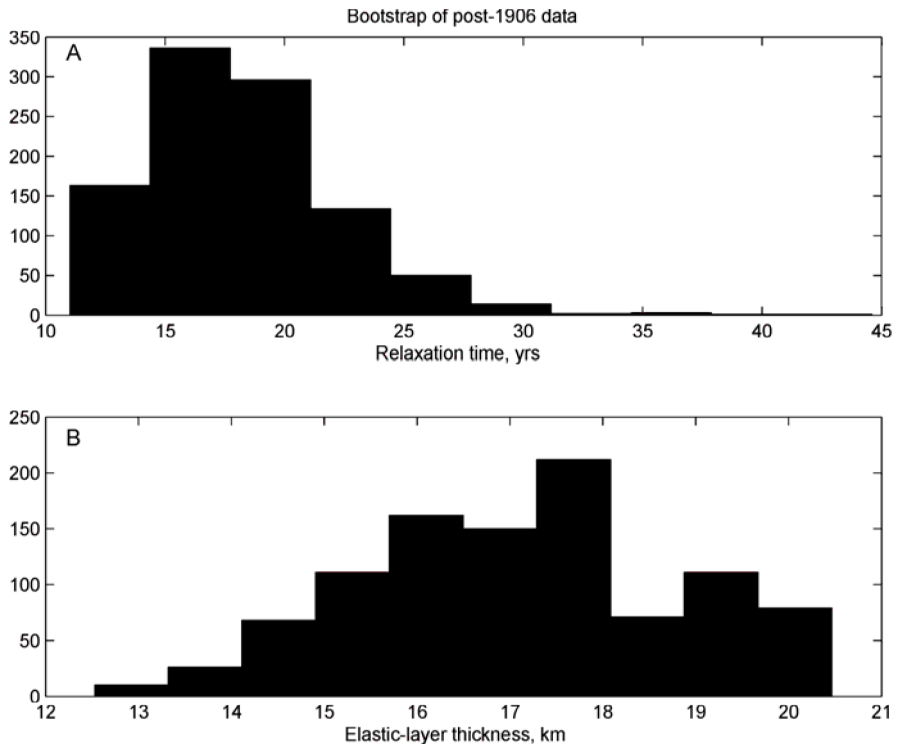

FIG. 12. Bootstrap results for post-1906 data in the San Francisco Bay area. A. Relaxation time. B. Elastic-layer thickness (1,000 bootstrap resamples).

lated annealing algorithm did not show evidence of local minima, so the remaining analysis was done using a Sequential Quadratic Programming method, with BFGS Hessian updates (e.g. Gill et al., 1981) within Matlab. The method allows upper and lower bounds to be placed on all parameters as well as generalized inequality constraints. The latter are needed because t_{HRC} is strictly bounded by $t_{HRC} \leq T_{HRC}$. In the context of the Savage and Prescott model, earthquakes are periodic, and it makes no sense for the elapsed time since the last event to exceed the average recurrence time. In addition, I have found it desirable to constrain the maximum coseismic slip on both the San Andreas and Hayward faults. This provides constraints of the form: $\dot{s}_{SAF} \cdot T_{SAF} \leq \Delta u_{SAF}^{max}$, and $\dot{s}_{HRC} \cdot T_{HRC} \leq \Delta u_{HRC}^{max}$. Noting that the coseismic slip should be interpreted as an average over the fault in this two-dimensional model, I set $\Delta u_{SAF}^{max} = 7.0$ meters, and $\Delta u_{HRC}^{max} = 3.0$ meters.

It should be noted that the GPS network does not extend very far west of the San Andreas fault. For this reason, the data do not adequately constrain the total motion across the plate boundary. A reasonable approach would be to include data from Pacific plate sites such as Hawaii. I chose simply to constrain the sum of the slip rates on all three faults to be no greater than 40 mm/yr (e.g. Argus and Gordon, 2001). This constraint significantly affects the solution; estimates without the cumulative slip constraint tended to put the maximum slip rate allowed on all three faults, exceeding the total displacement rate between the Sierra Nevada–Great Valley block and the Pacific plate.

The optimal solution is found for $H \sim 18.4$ km, $\tau_R \sim 34.5$ years, $T_{SAF} = 280$ years, $\dot{s}_{SAF} \sim 25$ mm/yr, $t_{HRC} = 225$ years, $T_{HRC} = 428.6$ years, and $\dot{s}_{HRC} \sim 7$ mm/yr. The Concord–Green Valley fault slips at $\dot{s}_{HRC} \sim 8$ mm/yr below 2.2 km. A surprising result is that the predicted recurrence time on the San Andreas is reasonable in the sense of requiring 7.0-meter slip events every 280 years. In comparison, Schwartz et al. (1998) suggested that the penultimate event on the north coast segment of the San Andreas occurred in the mid-1600s, possibly in the interval 1632–1659, corresponding to a recurrence interval of roughly 260 years. Also surprising is that the time since the last earthquake on the Hayward–

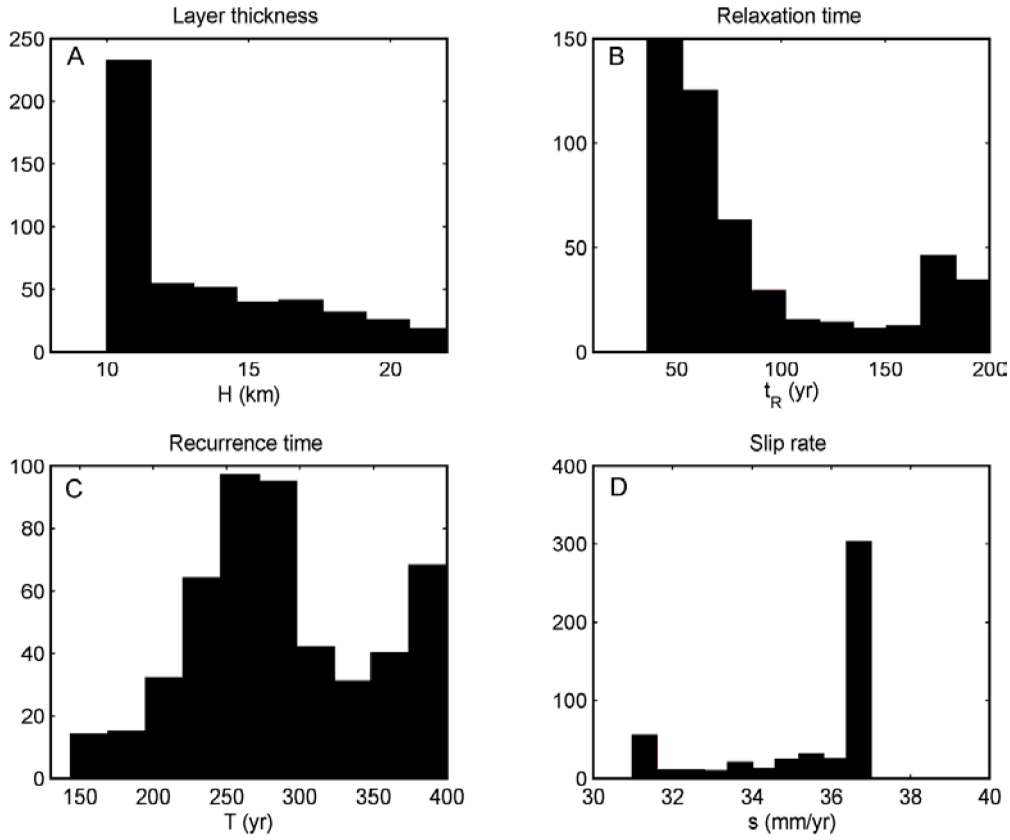

FIG. 13. Bootstrap results for SCEC data along the Carrizo Plain segment of the San Andreas fault. A. Elastic-layer thickness. B. Relaxation time. Note that 200 years was the upper bound considered. C. Recurrence time. Recurrence times in excess of 400 years were not considered, as these would lead to excessive coseismic slip. D. Slip rate.

Rodgers Creek fault is the minimum allowed, 225 years. A comparison of the model fit to the data sets is shown in Figure 15. Generally speaking, the data are fit quite well, with the possible exception of the strain rate in the first post-1906 epoch. The uncertainties in the post-1906 strain rates were actually decreased by a factor of two to ensure that these data are fairly weighted compared to the GPS velocities. Decreasing the uncertainties in the strain rates further to fit high strain rate in the immediate post-1906 epoch causes a very significant increase in the misfit to the modern GPS data. This is most likely a result of the large uncertainties in the triangulation data, but may also indicate that the physical model is inadequate.

How is it that the geodetic data have any capability of resolving the recurrence interval on the San Andreas fault? Recall that there are three times in the physical model: the time since the last major earthquake t, the asthenospheric relaxation time τ_R, and the recurrence interval T. For the San Andreas fault, we know t_{SAF} ~93 years *a priori*, and τ_R is reasonably well resolved by the post-1906 strain rate transient. The estimation is thus free to vary T in such a way as to optimize the fit to the velocity gradients near the San Andreas. Constraints on the maximum slip in the earthquake help to further tighten those constraints.

In order to determine how well the data constrain the model parameters, I ran 500 bootstrap resamples and optimizations, using the best-fitting model as the starting point of the optimization. As before, the residuals were resampled and added to the predicted data from the optimal model, in order to ensure that each observation point contributes to the solution. The results of the bootstrap are shown in Figure 16. The posterior distribution for recurrence time on the San Andreas fault, T_{SAF}, is quite broad, with a peak near the maximum allowed of (7000 mm)/(19 mm/yr) ~370 years. In contrast, the posterior distribution for recurrence time on the Hayward–Rodgers Creek fault, T_{HRC}, is bimodal, with prominent peaks near the minimum ~225 years and maximum allowed value (3000 mm)/(7 mm/yr)

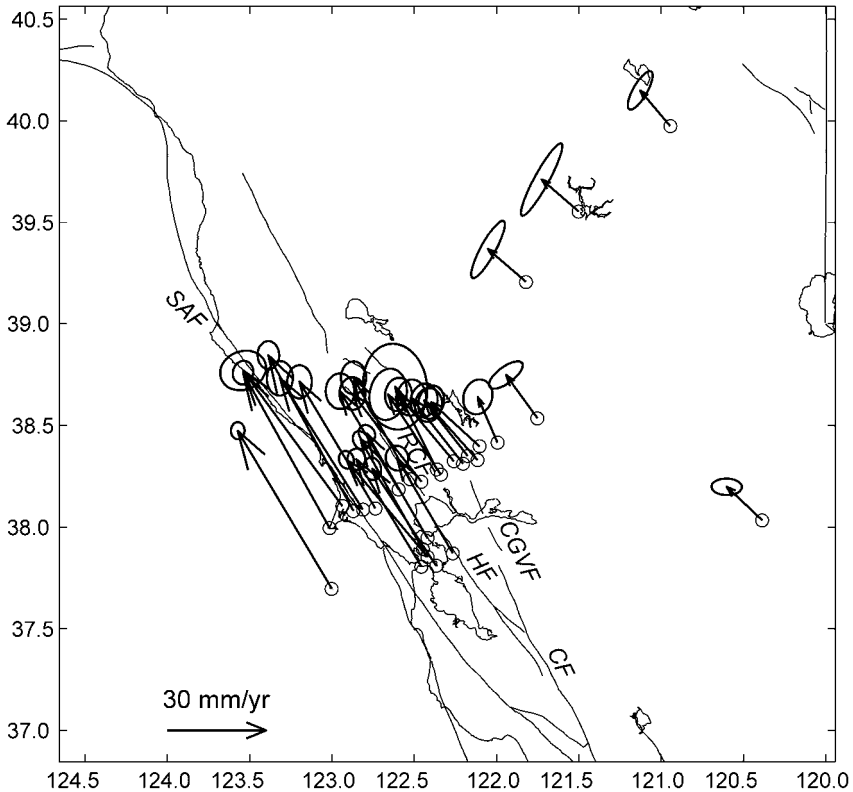

FIG. 14. GPS-derived velocities for the north San Francisco Bay region, after Prescott et al (2001). Abbreviations: SAF = San Andreas fault; HF = Hayward fault; CF = Calaveras fault; RGF = Rodgers Creek fault; CGVF = Concord–Green Valley fault.

TABLE 1. *A priori* Bounds on Parameters

Parameter	Symbol	Min	Max
Lithospheric thickness, km	H	10	30
Relaxation time, yr	τ_R	10	200
SAF recurrence interval, yr	T_{SAF}	100	500
Time since last Hayward event, yr	t_{HRC}	225	690
Hayward recurrence interval, yr	T_{HRC}	225	700
Green valley fault locking depth, km	d	0.5	15
SAF slip rate, m/y	$\dot{s}_{SAF}$	0.019	0.027
Hayward slip rate, m/yr	$\dot{s}_{HRC}$	0.007	0.013
Green valley slip rate, m/yr	$\dot{s}_{CGV}$	0.002	0.008

~ 428 years. The distributions for t_{HRC}, the time since the most recent Hayward–Rodgers Creek earthquake, is strongly concentrated near the minimum allowed range. The distribution of slip rates on the San Andreas and Hayward–Rodgers Creek faults are bimodal, with peaks at 19 mm/yr and 25

TABLE 2. Influence of Maximum Coseismic Slip on Estimated Parameters[1]

Parameter	$\Delta u_{SAF}^{max} = 5.5$ $\Delta u_{HRC}^{max} = 2.0$	$\Delta u_{SAF}^{max} = 7.0$ $\Delta u_{HRC}^{max} = 3.0$	$\Delta u_{SAF}^{max} = 10.0$ $\Delta u_{HRC}^{max} = 5.0$
Lithospheric thickness, H, km	15.0	18.4	22.0
Relaxation time, τ_R, yr	35.7	34.5	34.0
SAF recurrence interval, T_{SAF}, yr	220	280	337
Limiting interval, $\Delta u_{SAF}^{max}/\dot{s}_{SAF}$, yr	290	368	526
Time since last Hayward event, t_{HRC}, yr	225	225	225
Hayward recurrence interval, T_{HRC}, yr	285.7	428.6	700
Limiting interval, $\Delta u_{HRC}^{max}/\dot{s}_{HRC}$, yr	285	428	714
Green Valley fault locking depth, d, km	1.1	2.2	4.7
SAF slip rate, $\dot{s}_{SAF}$, m/yr	0.025	0.025	0.0249
Hayward slip rate, $\dot{s}_{HRC}$, m/yr	0.007	0.007	0.0071
Green valley slip rate, $\dot{s}_{CGV}$, m/yr	0.008	0.008	0.008

[1]Limiting interval is computed using the estimated slip rate for that fault, not the minimum slip rate that would yield a longer upper bound.

mm/yr (SAF) and 7 mm/yr and 13 mm/yr (HRC). These results still must be viewed with some caution, in that I have not demonstrated that the bootstrap optimizations were immune to local minima.

The bootstrap calculations suggest that the constraint on maximum coseismic slip does play a strong role in the results. To explore this further, I varied the maximum coseismic slip allowed on the two faults. The results (Table 2) demonstrate that the San Andreas recurrence interval is not fully controlled by the constraint on the maximum coseismic slip. In contrast, the recurrence interval on the Hayward fault is totally controlled by the maximum slip allowed (for a maximum slip of 10 meters the recurrence interval reaches the upper bound of 700 years). Notice also that the time since the last Hayward–Rodgers Creek event is always at the minimum value allowed (225 years). The fit to the data is slightly better for large, infrequent earthquakes.

Discussion

What has been learned from the modeling presented here? It seems clear that geodetic data should not be analyzed in a vacuum. The resolution of the data alone is insufficient to address the problems of greatest interest. However, when combined with prior information from geologic studies, GPS data appear to be able to resolve parameters of considerable interest such as the average recurrence interval between great earthquakes on the San Andreas fault. Using a simple model of a repeating dislocation rupturing an elastic plate overlying a Maxwell visco-elastic medium, I found an average recurrence interval of roughly 280 years on the north coast segment of the San Andreas fault. Although the uncertainties in this estimate are large, the result is in surprisingly good accordance with recent paleoseismic results (Schwartz et al., 1998) that suggest an event similar to 1906 in the mid 1600s.

The results for the Hayward–Rodgers Creek fault are also not unreasonable. According to the GPS data, the most recent event here occurred in ~1775, regardless of the estimated recurrence time. This result is not inconsistent with the paleoseismic finding that the most recent event on the Rodgers Creek fault took place in the interval 1670–1776

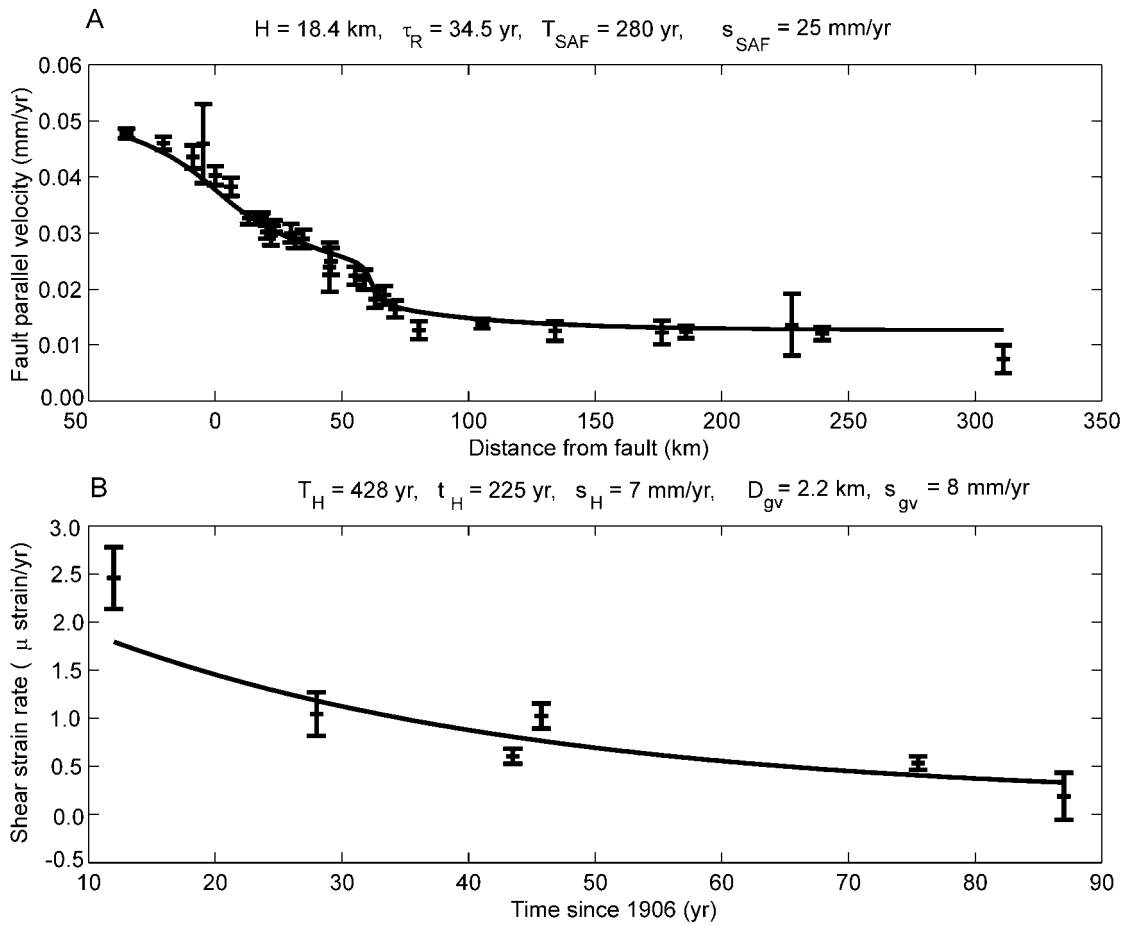

FIG. 15. Fit of model to north San Francisco Bay data. Maximum slip on Hayward fault is 3.0 m, and on the SAF is 7.0 m.

(Schwartz et al., 1993), and on the northern Hayward fault in 1640–1776 (HFPEG, 1999). The GPS data alone yield limited information about the average recurrence time on the Hayward–Rodgers Creek fault. However, adding the reasonable bound that slip not exceed 2 meters on average yields a recurrence interval of 285 years. The average slip in the 1868 Hayward fault earthquake was approximately 2 meters (Yu and Segall, 1996). In comparison, trenching at the El Cerrito site on the northern Hayward fault suggests a recurrence interval of possibly less than 270 years but no more than 710 years (HFPEG, 1999).

It should not need to be stated that earthquakes are neither periodic nor, especially in the case of the Hayward–Rodgers Creek faults, infinitely long. A two-dimensional model cannot describe the situation at a given trench site where ruptures mainly to the north or south of the site cause some offset in the trench. Nevertheless, the fact that the results from such a simple model are not unreasonable is encouraging. One useful attribute of the models explored here are that they are testable in the sense of predicting future behavior. Running the model forward in time to the next San Andreas earthquake yields the velocity distributions shown in Figure 17. Of course, a north Hayward–Rodgers Creek earthquake may occur prior to the next San Andreas event.

The Maxwell relaxation time is reasonably well estimated by the data. I find an optimal value of about 35 years, which corresponds to a viscosity of 1.6×10^{19} Pa-s. It should be noted that the estimates of all of the model parameters is only as good as the mechanical model used to interpret the data. If, as seems quite likely, there was afterslip on the San Andreas below the 1906 rupture zone, the estimate of the viscosity is some combination of the effects of afterslip and distributed

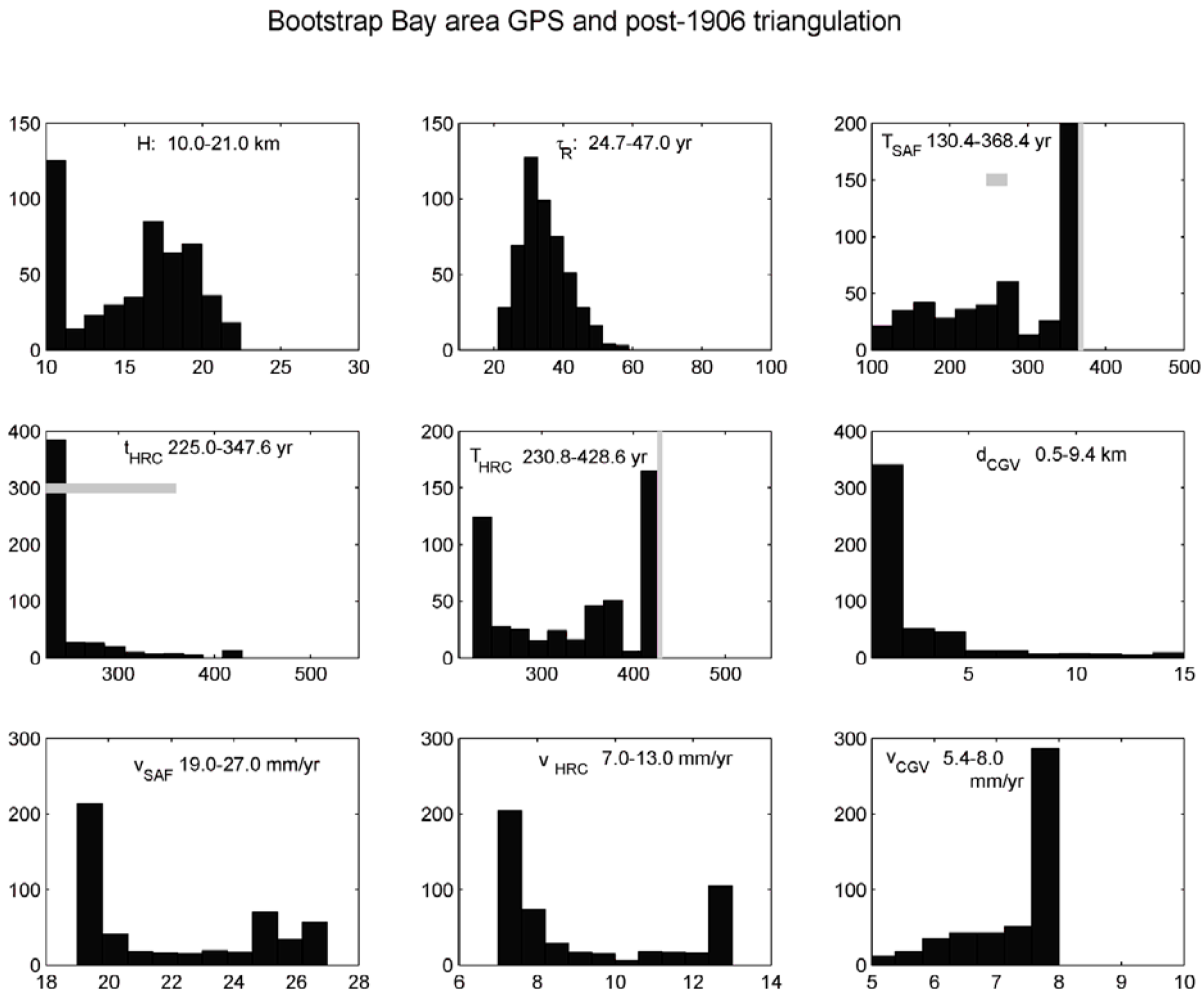

FIG. 16. Five hundred bootstrap estimates of model parameters fit to the north San Francisco Bay data; 90% confidence bounds are listed at the top of each panel. The vertical line in the histograms for recurrence times, T_{SAF}, and T_{HRC} show the upper bounds corresponding to the minimum slip rate and maximum allowed coseismic slip, respectively. The horizontal bar in the panel for the San Andreas recurrence time shows the preferred estimate from Schwartz et al. (1998). The horizontal bar in the panel for t_H, time since the last Hayward earthquake, shows the range of dates compatible with paleoseismic estimates of the penultimate Hayward–Rodgers Creek event.

relaxation. Li and Rice (1987) presented an approximate method for including post-seismic fault slip at constant resistive stress with a relaxing asthenosphere in the context of a repeating periodic earthquake sequence. Combining such an approach with appropriate constitutive laws for stable fault creep, as in Tse and Rice (1986), would presumably provide a more physically realistic description of fault behavior. Clearly, three-dimensional effects are also important, especially for earthquakes on the Rodgers Creek and Hayward faults. Finally, the effects of non-uniform elastic properties are known to bias interpretations based on simple homogeneous models. Elastic moduli increase with depth, which has the known effect of biasing the depth distribution of fault slip. Similarly, elastic properties may vary with lithology across the major fault zones, which themselves may represent zones of more compliant rock. Finite elements are certainly the most general way to compute forward models, but are not yet feasible for the optimization and bootstrap methods as computed here, which literally tested thousands of possible models.

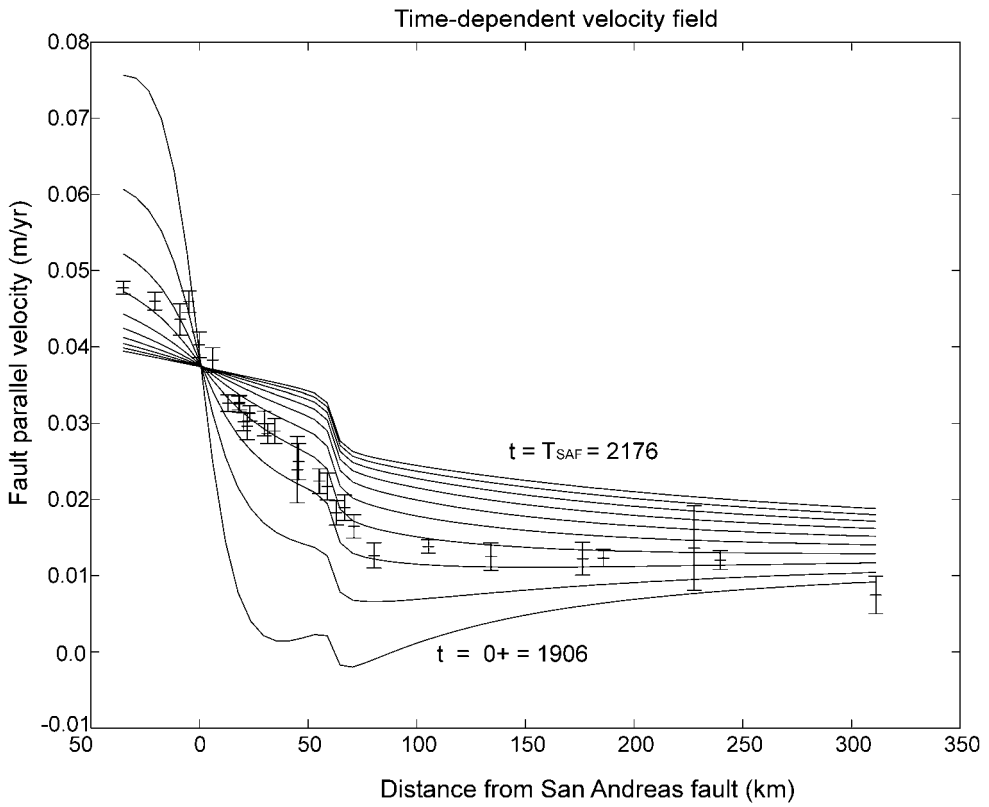

FIG. 17. Simulation of Bay Area velocity field as a function of time. Each line is separated by roughly 27 years.

Acknowledgments

George Thompson set a standard that geophysical models, no matter how elegant, must be consistent with geologic observations. This work was inspired by that example. I would like to thank Will Prescott for discussions about the Bay Area deformation measurements and Mark Matthews for many years ago introducing me to Bayes' theorem. Wayne Thatcher, Mark Murray, Jeff McGuire, and Peter Cervelli provided valuable comments at early stages in this study. I thank Jim Savage, Duncan Agnew, and Shelley Kenner for their thoughtful reviews. Gary Ernst and Simon Klemperer carefully edited the manuscript.

REFERENCES

Argus, D. F., and Gordon, R. G., 2001, Present tectonic motion across the Coast Ranges and San Andreas fault system in central California: Geological Society of America Bulletin, v. 113, p. 1580–1592.

Beroza, G. C., 1991, Near-source modeling of the Loma Prieta earthquake: Evidence for heterogeneous slip and implications for earthquake hazard: Bulletin of the Seismological Society of America, v. 81, p. 1603–1621.

Cohen, S. C., 1982, A multilayer model of time-dependent deformation following an earthquake on a strike-slip fault: Journal of Geophysical Research, v. 87, p. 5409–5421.

HFPEG (Hayward Fault Paleoearthquake Group), 1999, Timing of paleoearthquakes on the northern Hayward fault—Preliminary evidence in El Cerrito, California: U.S. Geological Survey, Open File Report 99-318.

Henstock, T. J., Levander, A., and Hole, J. A., 1997, Deformation in the lower crust of the San Andreas fault system in northern California: Science, v. 278, p. 650–653.

Feigl, K. L., King, R. W., and Jordan, T. H., 1990, Geodetic measurement of tectonic deformation in the Santa Maria fold and thrust belt, California: Journal of Geophysical Research, v. 95, p. 2679–2699.

Gill, P. E., Murray, W., and Wright, M. H., 1981, Practical optimization: London, UK, Academic Press, 401 p.

Grant, L. B. and Sieh, K., 1994, Paleoseismic evidence of clustered earthquakes on the San Andreas fault in the

Carrizo Plain, California: Journal of Geophysical Research, v. 99, p. 6819–6841.

Jackson, D. D., 1979, The use of *a priori* data to resolve the non-uniqueness in linear inversion: Geophysical Journal of the Royal Astronomical Society, v. 57, p. 137–157.

Johnson, H. O., Agnew, D. C., and Wyatt, F. K., 1994, Present-day crustal deformation in Southern California: Journal of Geophysical Research, v. 99, p. 23,951–23,974.

Kenner, S. J., and Segall, P., 2000, Postseismic deformation following the 1906 San Francisco earthquake: Journal of Geophysical Research, v. 105, p. 13,195–13,209.

_____, 2001, Lower crustal structure in northern California: Implications from strain-rate variations following the 1906 San Francisco earthquake: Journal of Geophysical Research, in review.

Lehner, F. K., Li, V. C., and Rice, J. R., 1981, Stress diffusion along rupturing plate boundaries: Journal of Geophysical Research, v. 86, p. 6155–6169.

Li, V. C., and Rice, J. R., 1987, Crustal deformation in great California earthquake cycles: Journal of Geophysical Research, v. 92, p. 11,533–11,551.

Lyzenga, G. A., Raefsky, A., and Mulligan, S. G., 1991, Models of recurrent strike-slip earthquake cycles and the state of crustal stress: Journal of Geophysical Research, v. 96, p. 21,623–21,640.

Matsu'ura, M., Jackson, D. D., and Cheng, A., 1986, Dislocation model for aseismic crustal deformation at Hollister, California: Journal of Geophysical Research, v. 91, p. 12,661–12,674.

Matthews, M. V., and Segall, P., Estimation of depth-dependent fault slip from measured surface deformation with application to the 1906 San Francisco earthquake: Journal of Geophysical Research, v. 98, p. 12,153–12,163.

Menke, W., 1989, Geophysical data analysis: Discrete inverse theory: San Diego, CA, Academic Press, 1989.

Minster, J. B., and Jordan, T. H., 1987, Vector constraints on western U.S. deformation from space geodesy, neotectonics, and plate motions: Journal of Geophysical Research, v. 92, p. 4798–4804.

Murray, M. H., and Segall, P., 2001, Modeling broadscale deformation in northern California and Nevada from plate motions and elastic strain accumulation: Geophysical Research Letters, in press.

Nur, A., and Mavko, G., 1974, Postseismic viscoelastic rebound: Science, v. 183, no. 4121, p. 204–206.

Parsons, T., and Hart, P. E., 1999, Dipping San Andreas and Hayward faults revealed beneath San Francisco Bay, California: Geology, v. 27, p. 839–842.

Prescott, W. H., Savage, J. C., Svarc, J. L., and Manaker, D., 2001, Deformation across the Pacific–North America plate boundary near San Francisco, California: Journal of Geophysical Research, v. 106, p. 6673–6682.

Pollitz, F. F., and Sacks, I. S., 1992, Modeling of postseismic relaxation following the great 1857 earthquake, southern California: Bulletin of the Seismological Society of America, v. 82, p. 454–480.

Reches, Z., Schubert, G., and Anderson, C., 1994, Modeling of periodic great earthquakes on the San Andreas fault; effects of nonlinear crustal rheology: Journal of Geophysical Research, v. 99, p. 21,983–22,000.

Rundle, J. B., 1986, An approach to modeling present-day deformation in southern California: Journal of Geophysical Research, v. 91, p. 1947–1959.

Savage, J. C., 1990, Equivalent strike-slip earthquake cycles in half-space and lithosphere-asthenosphere Earth models: Journal of Geophysical Research, v. 95, p. 4873–4879.

Savage, J. C., and Burford, R. O., 1970, Accumulation of tectonic strain in California: Bulletin of the Seismological Society of America, v. 60, p. 1877–1896.

Savage, J. C., and Prescott, W. H., 1978, Asthenosphere readjustment and the earthquake cycle: Journal of Geophysical Research, v. 83, p. 3369–3376.

Schwartz, D. P., Pantosti, D., Hecker, S., Okumara, K., Budding, K. E., and Powers, T., 1993, Late Holocene behavior and seismogenic potential of the Rodgers Creek fault zone, Sonoma County, California: California Division of Mines and Geology, Special Publication, v. 113, p. 393–398.

Schwartz, D. P., Pantosti, D., Okumara, K., Powers, T. J., and Hamilton, J. C., 1998, Paleoseismic investigations in the Santa Cruz mountains, California: Implications for recurrence of large-magnitude earthquakes on the San Andreas fault: Journal of Geophysical Research, v. 103, p. 17,985–18,001.

Sieh, K. E., and Jahns, R. H., 1984, Holocene activity of the San Andreas fault at Wallace Creek, California: Geological Society of America Bulletin, v. 95, p. 883–896.

Tarantola, A. and Valette, B., 1982, Generalized non-linear inverse problems solved using least squares criterion: Reviews of Geophysics and Space Physics, v. 20, p. 219–232.

Thatcher, W., 1975a, Strain accumulation and release mechanism of the 1906 San Francisco earthquake: Journal of Geophysical Research, v. 80, p. 4862–4872.

_____, 1975b, Strain accumulation on the northern San Andreas fault zone since 1906: Journal of Geophysical Research, v. 80, p. 4873–4880.

_____, 1983, Nonlinear strain buildup and the earthquake cycle on the San Andreas fault: Journal of Geophysical Research, v. 88, p. 5893–5902.

Toppozada, T. R., and Borchardt, G., 1998, Re-evaluation of the 1836 "Hayward fault" earthquake and the 1838 San Andreas fault earthquake: Bulletin of the Seismological Society of America, v. 88, p. 140–159.

Tse, S. T., and Rice, J. R., 1986, Crustal earthquake instability in relation to the depth variation of frictional slip

properties: Journal of Geophysical Research, v. 91, p. 9452–9472.

Williams, S. D. P., Svarc, J. L., Lisowski, M., and Prescott, W. H., 1994, GPS-measured rates of deformation in the northern San Francisco Bay region, California, 1990–1993: Geophysical Research Letters, v. 21, p. 1511–1514.

WGCEP (Working Group on California Earthquake Probabilities), 1988, Probabilities of large earthquakes occurring in California on the San Andreas fault: U.S. Geological Survey, Open File Report, 88-398.

_____, 1995, Seismic hazards in southern California: Probable earthquakes,1994–2024: Bulletin of the Seismological Society of America, v. 85, p. 379–439.

_____, 1999, Earthquake probabilities in the San Francisco Bay Region: 2000–2030—A summary of findings: U.S. Geological Survey, Open File Report, 99–517.

Yu, E., and Segall, P., 1996, Slip in the 1868 Hayward Earthquake from the analysis of historical triangulation data: Journal of Geophysical Research, v. 101, p. 16,101–16,118.